ICHEP94 Ref. GSL0389 **CLEO CONF 94-4**
Submitted to PA 21,2 Pl 9,19

Search for $B \to K\ell^+\ell^-$ and $B \to K^*\ell^+\ell^-$ decays.

R. Balest,[1] K. Cho,[1] W.T. Ford,[1] D.R. Johnson,[1] K. Lingel,[1] M. Lohner,[1] P. Rankin,[1] J.G. Smith,[1] J.P. Alexander,[2] C. Bebek,[2] K. Berkelman,[2] K. Bloom,[2] T.E. Browder,[2*] D.G. Cassel,[2] H.A. Cho,[2] D.M. Coffman,[2] D.S. Crowcroft,[2] P.S. Drell,[2] D. Dumas,[2] R. Ehrlich,[2] P. Gaidarev,[2] M. Garcia-Sciveres,[2] B. Geiser,[2] B. Gittelman,[2] S.W. Gray,[2] D.L. Hartill,[2] B.K. Heltsley,[2] S. Henderson,[2] C.D. Jones,[2] S.L. Jones,[2] J. Kandaswamy,[2] N. Katayama,[2] P.C. Kim,[2] D.L. Kreinick,[2] G.S. Ludwig,[2] J. Masui,[2] J. Mevissen,[2] N.B. Mistry,[2] C.R. Ng,[2] E. Nordberg,[2] J.R. Patterson,[2] D. Peterson,[2] D. Riley,[2] S. Salman,[2] M. Sapper,[2] F. Würthwein,[2] P. Avery,[3] A. Freyberger,[3] J. Rodriguez,[3] S. Yang,[3] J. Yelton,[3] D. Cinabro,[4] T. Liu,[4] M. Saulnier,[4] R. Wilson,[4] H. Yamamoto,[4] T. Bergfeld,[5] B.I. Eisenstein,[5] G. Gollin,[5] B. Ong,[5] M. Palmer,[5] M. Selen,[5] J. J. Thaler,[5] K.W. Edwards,[6] M. Ogg,[6] A. Bellerive,[7] D.I. Britton,[7] E.R.F. Hyatt,[7] D.B. MacFarlane,[7] P.M. Patel,[7] B. Spaan,[7] A.J. Sadoff,[8] R. Ammar,[9] P. Baringer,[9] A. Bean,[9] D. Besson,[9] D. Coppage,[9] N. Copty,[9] R. Davis,[9] N. Hancock,[9] M. Kelly,[9] S. Kotov,[9] I. Kravchenko,[9] N. Kwak,[9] H. Lam,[9] Y. Kubota,[10] M. Lattery,[10] M. Momayezi,[10] J.K. Nelson,[10] S. Patton,[10] R. Poling,[10] V. Savinov,[10] S. Schrenk,[10] R. Wang,[10] M.S. Alam,[11] I.J. Kim,[11] Z. Ling,[11] A.H. Mahmood,[11] J.J. O'Neill,[11] H. Severini,[11] C.R. Sun,[11] F. Wappler,[11] G. Crawford,[12] C. M. Daubenmier,[12] R. Fulton,[12] D. Fujino,[12] K.K. Gan,[12] K. Honscheid,[12] H. Kagan,[12] R. Kass,[12] J. Lee,[12] R. Malchow,[12] Y. Skovpen,[12†] M. Sung,[12] C. White,[12] M.M. Zoeller,[12] F. Butler,[13] X. Fu,[13] B. Nemati,[13] W.R. Ross,[13] P. Skubic,[13] M. Wood,[13] M. Bishai,[14] J. Fast,[14] E. Gerndt,[14] R.L. McIlwain,[14] T. Miao,[14] D.H. Miller,[14] M. Modesitt,[14] D. Payne,[14] E.I. Shibata,[14] I.P.J. Shipsey,[14] P.N. Wang,[14] M. Battle,[15] J. Ernst,[15] L. Gibbons,[15] Y. Kwon,[15] S. Roberts,[15] E.H. Thorndike,[15] C.H. Wang,[15] J. Dominick,[16] M. Lambrecht,[16] S. Sanghera,[16] V. Shelkov,[16] T. Skwarnicki,[16] R. Stroynowski,[16] I. Volobouev,[16] G. Wei,[16] P. Zadorozhny,[16] M. Artuso,[17] M. Gao,[17] M. Goldberg,[17] D. He,[17] N. Horwitz,[17] R. Kennett,[17] G.C. Moneti,[17] R. Mountain,[17] F. Muheim,[17] Y. Mukhin,[17] S. Playfer,[17] Y. Rozen,[17] S. Stone,[17] X. Xing,[17] G. Zhu,[17] J. Bartelt,[18] S.E. Csorna,[18] Z. Egyed,[18] V. Jain,[18] D. Gibaut,[19] K. Kinoshita,[19] P. Pomianowski,[19] B. Barish,[20] M. Chadha,[20] S. Chan,[20] D.F. Cowen,[20] G. Eigen,[20] J.S. Miller,[20] C. O'Grady,[20] J. Urheim,[20] A.J. Weinstein,[20] M. Athanas,[21] W. Brower,[21] G. Masek,[21] H.P. Paar,[21] J. Gronberg,[22] R. Kutschke,[22] S. Menary,[22] R.J. Morrison,[22] S. Nakanishi,[22] H.N. Nelson,[22] T.K. Nelson,[22] C. Qiao,[22] J.D. Richman,[22] A. Ryd,[22] H. Tajima,[22] D. Sperka,[22] and M.S. Witherell[22]

(CLEO Collaboration)

[1]*University of Colorado, Boulder, Colorado 80309-0390*
[2]*Cornell University, Ithaca, New York 14853*
[3]*University of Florida, Gainesville, Florida 32611*
[4]*Harvard University, Cambridge, Massachusetts 02138*
[5]*University of Illinois, Champaign-Urbana, Illinois, 61801*
[6]*Carleton University, Ottawa, Ontario K1S 5B6 and the Institute of Particle Physics, Canada*
[7]*McGill University, Montréal, Québec H3A 2T8 and the Institute of Particle Physics, Canada*
[8]*Ithaca College, Ithaca, New York 14850*
[9]*University of Kansas, Lawrence, Kansas 66045*
[10]*University of Minnesota, Minneapolis, Minnesota 55455*
[11]*State University of New York at Albany, Albany, New York 12222*
[12]*Ohio State University, Columbus, Ohio, 43210*
[13]*University of Oklahoma, Norman, Oklahoma 73019*
[14]*Purdue University, West Lafayette, Indiana 47907*
[15]*University of Rochester, Rochester, New York 14627*
[16]*Southern Methodist University, Dallas, Texas 75275*
[17]*Syracuse University, Syracuse, New York 13244*
[18]*Vanderbilt University, Nashville, Tennessee 37235*
[19]*Virginia Polytechnic Institute and State University, Blacksburg, Virginia, 24061*
[20]*California Institute of Technology, Pasadena, California 91125*
[21]*University of California, San Diego, La Jolla, California 92093*
[22]*University of California, Santa Barbara, California 93106*

Abstract

We have searched for the flavor-changing-neutral-current (FCNC) decays $B \to K\ell^+\ell^-$ and $B \to K^*\ell^+\ell^-$. Using a data sample of 2.17×10^6 $B\bar{B}$ events, we find 90% confidence level upper limits on the branching ratios: BR($B^- \to K^-e^+e^-$) $< 1.2\times 10^{-5}$, BR($\bar{B}^0 \to \bar{K}^{*0}e^+e^-$) $< 1.6\times 10^{-5}$, BR($B^- \to K^-\mu^+\mu^-$) $< 0.9\times 10^{-5}$, BR($\bar{B}^0 \to \bar{K}^{*0}\mu^+\mu^-$) $< 3.1\times 10^{-5}$, BR($B^- \to K^-e^\pm\mu^\mp$) $< 1.2\times 10^{-5}$, and BR($\bar{B}^0 \to \bar{K}^{*0}e^\pm\mu^\mp$) $< 2.7\times 10^{-5}$. The limit on $\bar{B}^0 \to \bar{K}^{*0}e^+e^-$ is within a factor of 3 of the branching ratio predicted by the Standard Model.

*Permanent address: University of Hawaii at Manoa

†Permanent address: INP, Novosibirsk, Russia

In the Standard Model (SM), flavor-changing-neutral-current (FCNC) decays are forbidden at tree level, but are allowed through higher order Feynman diagrams such as electroweak penguin or weak box diagrams. Because of the low rate expected within the SM, and because high-mass particles can contribute to loop and box diagrams, these processes are sensitive to non-SM physics. One such process, $B \to K^*(892)\gamma$ decay, has previously been observed by the CLEO collaboration [1]. There has yet to be any experimental evidence for FCNC processes with lepton pairs in the final state. There has been considerable theoretical interest in such decays [2]- [5]. These decays have smaller QCD corrections [3] than $b \to s\gamma$ and also are sensitive to additional non-SM physics such as tree-level flavor-changing neutral currents. In this paper, we present results on the search for the exclusive FCNC decays $B \to K^{(*)}\ell^+\ell^-$ and the SM-forbidden decays $B \to K^{(*)}e^\pm\mu^\mp$. ($K^{(*)}$ denotes either $K^\pm$ or $K^*(892)^0$.) The SM-allowed diagrams for these decays are shown in Fig. 1.

The data sample used in this analysis consists of $e^+e^- \to \Upsilon(4S) \to B\bar{B}$ events recorded with the CLEO-II detector [6] at the Cornell Electron Storage Ring (CESR). The integrated luminosity of the data set analyzed is 2.03 fb^{-1}, corresponding to the production of 2.17 million $B\bar{B}$ pairs. For the $B \to K^*\ell^+\ell^-$ mode, only the $K^{*0} \to K^\pm\pi^\mp$ channel is used. The final states considered here all contain two leptons and 1 or 2 additional charged tracks from the interaction point, with no neutral particles or secondary vertices. The signal events thus have a good detection efficiency and very small combinatoric backgrounds.

We select events passing standard hadronic event criteria, and further require that they contain at least 4 charged tracks. The tracks used to form the B candidate must be well-fit tracks coming from the interaction point. The electron candidates are required to have momenta greater than 0.6 GeV/c and a high likelihood of being an electron based on E/p, dE/dx, track-cluster matching, and shower shape and width in the crystal calorimeter [7]. The muon candidates are required to penetrate at least 3 interaction lengths in the muon absorber and have momenta greater than 1.0 GeV/c. The hadron selection makes conservative use of dE/dx and time-of-flight by requiring 3σ consistency in either device. The K^* candidate is required to have invariant mass of the $K\pi$ system within 0.1 GeV of the $K^*(892)^0$ mass.

To suppress hadrons misidentified as leptons ("fakes") and leptons from secondary decay of B mesons (*i.e.,* $b \to c \to s\ell\nu$) we require that one of the two leptons pass an additional cut (tight lepton cut). For a tight electron, we require a momentum cut of $p > 1.3$ GeV/c. The efficiency loss from the additional momentum cut is small. For a tight muon, we require a penetration depth of 5 interaction lengths and $p > 1.4$ GeV/c.

The lepton and hadron candidate tracks are combined to make a B candidate. Since the $\Upsilon(4S)$ resonance is below $B\bar{B}\pi$ threshold, all B mesons have energy $E_B = E_{\rm beam}$ and fixed momentum $p \approx 300$ MeV/c. We define two variables which makes use of these constraints: energy difference

$$\Delta E = \sum_i E_i \; - E_{\rm beam},$$

where E_i is the energy of the i-th daughter of the B candidate, and beam-constrained mass

$$M_B = \sqrt{E_{\rm beam}^2 - \left(\sum_i \vec{p}_i\right)^2}\;.$$

Only if an event has a B candidate with $|\Delta E| < 0.25$ GeV and $M_B > 5.2$ GeV, is it further considered. If an event has more than one such candidate for a given decay mode, the entry with the smallest $|\Delta E|$ is selected, thus allowing at most one entry per decay mode per event. To determine the signal yield and estimate the background therein, we define the signal region as the product of 2.5σ intervals in $\Delta E \otimes M_B$ space, where $\sigma(\Delta E)$ and $\sigma(M_B)$ are measured from signal Monte Carlo (MC). The range of the signal region in $\Delta E \otimes M_B$ is given in Table I for each mode.

In addition to the electroweak penguin and box diagram processes, the signal events have significant contributions from the decays $B \to \psi K^{(*)}$ and $B \to \psi' K^{(*)}$ where $\psi(\psi')$ decays into $\ell^+\ell^-$. We suppress these by rejecting events which have $2.9 \leq m_{\ell\ell} \leq 3.2$ GeV or $3.5 \leq m_{\ell\ell} \leq 3.8$ GeV.

For each B decay mode analyzed, we generated 10^4 MC events with full detector simulation. The signal MC events are generated according to a 3-body phase-space distribution. The background studies also use MC events. Since the expected number of background events is very small, we need a large initial sample to properly assess the features of the backgrounds. Therefore, we use a fast, parametric MC simulation of the CLEO experiment to make a large number of background MC events. We select events at the generator level, requiring that each event have at least two leptons of opposite charge with momenta of $p \geq 1.3$ GeV/c and $p \geq 0.6$ GeV/c. We have generated background MC samples equivalent to $\sim 3.8 \times 10^8$ $q\bar{q}$ continuum events and $\sim 7.5 \times 10^7$ $B\bar{B}$ events. These are almost 60 and 35 times larger than the data sample used in the analysis, respectively. In addition, we generated 1.1×10^7 continuum events without the generator-level preselection to measure the sample-size reduction that the di-lepton selection imposes on continuum events. The sample-size reduction factor for $B\bar{B}$ events is measured using generic CLEO MC events.

The generic $q\bar{q}$ and $B\bar{B}$ MC samples are also used to study the effect of fake leptons. The estimated number of background events at the end of the pre-selection procedure described thus far is summarized in Table II. In general, we note that the backgrounds involving fakes are more severe in the muon modes than in the electron modes, and in the $q\bar{q}$ continuum events than in the $B\bar{B}$ events. The background from fake leptons is comparable to or larger than that from correctly identified leptons. Therefore, fakes must be considered in the cut optimization.

As seen in Table II, the majority of backgrounds at this point of the analysis are from $q\bar{q}$ continuum. Since $B\bar{B}$ events have decay products relatively evenly distributed in space, while $q\bar{q}$ continuum events are jet-like, we use event shape variables to suppress continuum background. The variables used are R_2, $S_\perp$, and cosine of thrust angle ($\cos\theta_{\mathrm{T}}$); the meanings and definitions of these are:

- R_2: The normalized second Fox-Wolfram moment [8]. The value of R_2 lies between 0 (spherical) and 1 (jet-like). For $B\bar{B}$ events, R_2 tends to be small and for $q\bar{q}$, large. Figure 2(a) shows the R_2 distribution of the signal MC events and continuum MC events.

- $\cos\theta_{\mathrm{T}}$: The angle θ_{T} is between the thrust axis of the B candidate tracks and the thrust axis of the rest of the event, including charged tracks and neutral clusters. This variable has a meaning only if there is a well-defined axis in the event. Therefore we remove events only if the thrust of the B is larger than 0.9 and $\cos\theta_{\mathrm{T}}$ fails the cut. Figure 2(b) shows the thrust(B) distribution of the signal MC events and continuum

MC events and Figure 2(c) shows the $\cos\theta_{\rm T}$ distribution of events with thrust(B) > 0.9. Because of the jet-like event shape, $q\bar{q}$ events have $\cos\theta_{\rm T}$ near ± 1 while the signal events have $\cos\theta_{\rm T}$ more evenly distributed.

- $S_\perp$: This variable is defined as the sum of the magnitudes of the momentum vectors transverse to the thrust axis of the B candidate tracks, divided by the sum of the magnitudes of the momenta of all tracks. The tracks from the B candidate are excluded both from the numerator and the denominator. As with $\cos\theta_{\rm T}$, we compute $S_\perp$ only if the thrust of the B is larger than 0.9. Figure 2(d) shows the $S_\perp$ distribution of the signal MC events and continuum MC events. The signal MC events have large $S_\perp$, while the $q\bar{q}$ MC events have small $S_\perp$.

In evaluating the shape variables $S_\perp$ and $\cos\theta_{\rm T}$ we include all charged particles found in the drift chamber that satisfy track-quality cuts, and all shower clusters found in the CsI calorimeter not matched to any drift chamber tracks.

The cuts on shape variables are determined from a bootstrap method [9]. A fraction of the background MC event sample is randomly selected such that its sample size corresponds approximately to that of the CLEO data set used in this analysis, *i.e.* 2×10^6 $B\bar{B}$ and 6×10^6 $q\bar{q}$ events. We made 100 partial data sets. Each partial set represents a toy experiment of measuring the upper limit of the FCNC decays, because we did not include any signal MC events. The signal MC events are used to determine the efficiencies for each set of cuts used in the toy experiments. The cut values, defined as lattice points in the $R_2 \otimes \cos\theta_{\rm T} \otimes S_\perp$ space, are listed below.

$$R_2 \ : \ \text{no cut}, < 0.5, < 0.45, < 0.4, < 0.35, < 0.3, < 0.25$$
$$|\cos\theta_{\rm T}| \ : \ \text{no cut}, < 0.9, < 0.8$$
$$S_\perp \ : \ \text{no cut}, > 0.2, > 0.4$$

We examine each combination of R_2, $\cos\theta_{\rm T}$, and $S_\perp$ cuts. After 100 trials, we average the measured upper limits for each combination of shape variable cuts. The combination which gives the best averaged upper limit is taken as representing the optimal cuts. The cut values are summarized in Table III, along with the signal efficiencies for the corresponding cuts. The estimated backgrounds from both correct and fake lepton events after the shape variable cuts are also shown in Table III and are about 1 event or less for each mode. Note that the estimated background from $q\bar{q}$, which was the dominant background source before the shape cuts, is now less than the background from $B\bar{B}$. The major background source is $B\bar{B}$ events in which both B mesons decay semileptonically. At this time, we are using no cuts designed to suppress $B\bar{B}$ background.

As a check on procedures, we measured the branching ratios of $B \to \psi K^{(*)}$ decays in data with the same selection criteria. We obtain $B \to \psi K^{(*)}$ branching ratios which are consistent with the measurements reported in Ref. [10].

The efficiencies shown in Table III are obtained from MC signal samples generated according to 3-body phase space (3BPS). Of course, for a general search for non-SM physics, we do not know the appropriate matrix element. However if the detection efficiency is uniform over the Dalitz plot of the final state particles, then the average efficiency will not depend on decay dynamics. Figures 3(a),(b) show the Dalitz plots of the events generated according to 3BPS in Ke^+e^- and in $K^*e^+e^-$ modes and Figs. 3(c),(d) show the corresponding plots for the detected events. We note that the detection efficiencies are almost uniform over the accepted region, except for regions with zero acceptance due to momentum cuts and ψ and ψ' veto. We use the differential decay rate $d\Gamma_{B\to K^{(*)}\ell\ell}/dm^2_{\ell\ell}$ calculated by Ali *et al.* [4] to determine the difference in efficiency between 3BPS and SM. Figure 4(a) shows the distribution of m^2_{ee}/m^2_B in the $K^-e^+e^-$ mode as generated by MC using 3BPS and Fig. 4(b) shows the m^2_{ee}/m^2_B distribution according to an SM-based phenomenological model in Ref. [4]. The hatched regions represent those removed by ψ and ψ' veto. We find that for the $K^-\ell^+\ell^-$ final state, the SM distribution is very similar to the 3BPS and the effect of the difference between 3BPS and SM on the efficiency measurement is small compared to other systematic effects.

For the $K^*\ell^+\ell^-$ mode, however, the situation is quite different. Figure 4(c) shows the distribution of m^2_{ee}/m^2_B in the $K^*e^+e^-$ mode from 3BPS and Fig. 4(d) shows the m^2_{ee}/m^2_B distribution according to an SM-based model in Ref. [4]. It is clear from Fig. 4(d) that unlike 3BPS or the $K^-\ell^+\ell^-$ mode, the SM distribution of $K^*\ell^+\ell^-$ has a singularity of $1/m^2_{\ell\ell}$ as $m^2_{\ell\ell}\to 0$. (The total decay rate remains finite because there is a cut-off at $m^2_{\ell\ell}=4m^2_\ell$.) As seen in Fig. 3(c)-(d), there is a slight drop of efficiency in the low $m^2_{\ell\ell}$ region. When convoluted with the SM singularity of $1/m^2_{\ell\ell}$, this effect causes a decrease in the overall efficiency relative to the 3BPS value. We find the efficiency drop to be 15% for $K^*e^+e^-$. The $K^*\mu^+\mu^-$ mode has a higher momentum threshold for muon selection, thus increasing the efficiency loss in the low $m^2_{\mu\mu}$ region. Because of a higher μ mass cut-off in $m_{\mu\mu}$, however, the $1/m^2_{\ell\ell}$ singularity is less significant in $K^*\mu^+\mu^-$ than in $K^*e^+e^-$. Therefore, the net effect is similar in both $K^*e^+e^-$ and $K^*\mu^+\mu^-$ modes.

Since the $1/m^2_{\ell\ell}$ singularity given by the SM might also occur in non-SM models, but stronger singularities seem unlikely, we use the SM efficiencies for the $K^*e^+e^-$ and $K^*\mu^+\mu^-$ modes. For the other modes, we use 3BPS efficiencies (which are essentially the same as SM efficiencies in any case).

Figures 5, 6, and 7 show the scatter plots of ΔE *vs.* M_B, both for the CLEO data and for the signal MC events in $K^{(*)}e^+e^-$, $K^{(*)}\mu^+\mu^-$, and $K^{(*)}e^\pm\mu^\mp$ modes, respectively. The signal region is shown as a rectangular box in the corresponding scatter plot. The observed number of events in the signal region is summarized in Table IV. As seen in the table, 1 event is observed in $\bar{K}^{*0}e^\pm\mu^\mp$ channel and 2 events each in $K^-e^+e^-$ and $K^-e^\pm\mu^\mp$ channels, while no events are seen in $\bar{K}^{*0}e^+e^-$, $K^-\mu^+\mu^-$, and $\bar{K}^{*0}\mu^+\mu^-$ modes.

Since we find no compelling evidence for signals, we determine the upper limits for the corresponding branching ratios using a Poisson probability distribution. Taking a conservative approach, all observed events in the signal region are regarded as potential signal events and the signal efficiencies measured from MC are reduced by the amount of systematic uncertainties. The systematic uncertainties related to the efficiency measurement are of two types: experimental and theoretical. Experimental systematic uncertainties are well understood; these are mostly in common with other similar CLEO analyses and consist of uncertainties in lepton and hadron identification (ID), beam energy fluctuations, statistical errors in efficiency calculations, etc. Theoretical systematic uncertainties are specific to this analysis.

The systematic uncertainty in lepton ID is estimated to be 3%. Therefore, with two leptons in the final state, we take 6% as the systematic uncertainty due to lepton ID. We use hadron ID devices, dE/dx and time-of-flight, only to require 3σ consistency in either devices and take 5% as a conservative estimate of systematic uncertainty in hadron ID efficiency. Since we use 2.5σ intervals for the signal region with a typical value of $\sigma(M_B) \sim 2.5$ MeV, we estimate a 1σ variation in beam energy affects the efficiency only at a level of 5% . We have used 10^4 signal MC events for each mode to calculate efficiency. If the efficiency is low, the statistical error in the efficiency is dominated by the uncertainty in the number of detected events. In our analyses, the lowest efficiency is in $K^*\mu^+\mu^-$ mode with $\varepsilon \approx 5\%$. This gives a fractional uncertainty of $1/\sqrt{500} \approx 5\%$. Combining all these contributions in quadrature, we estimate that the experimental systematic error is 10%.

We take the efficiency difference of 15% between 3BPS and SM as the measure of systematic error due to model-dependence. Combining 15% systematic uncertainty from model-dependence and 10% from other sources, we conclude that the systematic uncertainty is at most 20%. To calculate the upper limits, we reduce the efficiency of all modes by 20% to conservatively take systematic effects into account. The upper limits on the branching ratios at 90% confidence level, allowing for the systematic uncertainties, are summarized in Table IV.

In conclusion, we have searched for the exclusive FCNC decays $B \to K^{(*)}e^+e^-$, $B \to K^{(*)}\mu^+\mu^-$, and lepton-number-nonconserving decays $B \to K^{(*)}e^\pm\mu^\mp$. We find no evidence for signals and compute the upper limits for the corresponding branching ratios. Table IV compares the theoretical predictions, the previously published upper limits, and the results from this analysis. The new upper limits on $K^{(*)}e^+e^-$ and $K^{(*)}e^\pm\mu^\mp$ modes are significantly more restrictive than previous results, as is the upper limit on $K^-\mu^+\mu^-$. The limit on $\bar{B}^0 \to \bar{K}^{*0}e^+e^-$ is within a factor of 3 of the branching ratio calculated by A. Ali *et al.* [5] based on the Standard Model.

We gratefully acknowledge the effort of the CESR staff in providing us with excellent luminosity and running conditions. This work was supported by the National Science Foundation, the U.S. Dept. of Energy, the Heisenberg Foundation, the SSC Fellowship program of TNRLC, Natural Sciences and Engineering Research Council of Canada, and the A.P. Sloan Foundation.

REFERENCES

[1] R. Ammar *et al.* (CLEO collaboration), Phys. Rev. Lett. **71**, 674 (1993).

[2] M. Gourdin, Phys. Lett. B **316**, 578 (1993); N.G. Deshpande, K. Panose, and J. Trampetic, Phys. Lett. B **308**, 322 (1993); P.J. O'Donnell, M. Sutherland, and H.K.K. Tung, Phys. Rev. D **46**, 4091 (1992); B. Grinstein, M.J. Savage, and M.B. Wise, Nucl. Phys. B **319**, 271 (1989); N.G. Deshpande and J. Trampetic, Phys. Rev. Lett. **60**, 2583 (1988); W-S. Hou, R.S. Willey, and A. Soni, Phys. Rev. Lett. **58**, 1608 (1987);

[3] R. Grigjanis, P.J. O'Donnell, M. Sutherland, and H. Navelet, Phys. Lett. B**223**, 239 (1989).

[4] A. Ali and T. Mannel, Phys. Lett. B**264**, 447 (1991).

[5] A. Ali, C. Greub, and T. Mannel, DESY 93-016.

[6] Y. Kubota *et al.* (CLEO collaboration), Nucl. Instrum. Methods Phys. Res., A**320**, 66 (1992).

[7] For details, see C. H. Wang, Ph.D. Thesis, Univ. of Rochester, (1993); M. Battle, Ph.D. Thesis, Univ. of Rochester, (1994).

[8] G. Fox and S. Wolfram, Phys. Rev. Lett. **41**, 1581 (1978).

[9] B. Efron, *The jackknife, the bootstrap, and other resampling plans*, (1982).

[10] M. S. Alam *et al.* (CLEO collaboration), CLNS 94/1270.

[11] K. Hikasa *et al.* (Particle Data Group), Phys. Rev. D**45**, (1992).

[12] CDF has reported a preliminary new limit of 3.2×10^{-5} for $B \to K\mu^+\mu^-$ at the *1994 Meeting of the American Physical Society*, Crystal City, VA, April 1994.

TABLE I. M_B and ΔE intervals which define the signal region for each FCNC decay mode: the signal regions are the product of 2.5σ intervals in $\Delta E \otimes M_B$ space, where $\sigma(\Delta E)$ and $\sigma(M_B)$ are measured from signal Monte Carlo (MC).

decay mode	$\pm 2.5\sigma_{M_B}$ (GeV)	$\pm 2.5\sigma_{\Delta E}$ (MeV)
$K^- e^+ e^-$	(5.2735, 5.2863)	(-68.5, 53.2)
$\bar{K}^{*0} e^+ e^-$	(5.2733, 5.2865)	(-61.9, 41.6)
$K^- \mu^+ \mu^-$	(5.2737, 5.2863)	(-60.6, 47.9)
$\bar{K}^{*0} \mu^+ \mu^-$	(5.2738, 5.2864)	(-49.9, 35.5)
$K^- e^\pm \mu^\mp$	(5.2737, 5.2862)	(-60.6, 46.1)
$\bar{K}^{*0} e^\pm \mu^\mp$	(5.2734, 5.2866)	(-57.8, 39.6)

TABLE II. Expected background per mode before shape variable cuts. The backgrounds are estimated from MC.

mode	from $B\bar{B}$		from $q\bar{q}$	
	correct	fake	correct	fake
$K^- e^+ e^-$	0.35	0.03	1.23	0.36
$\bar{K}^{*0} e^+ e^-$	0.83	0.11	0.71	0.48
$K^- \mu^+ \mu^-$	0.30	0.21	0.58	2.79
$\bar{K}^{*0} \mu^+ \mu^-$	0.35	0.29	0.34	1.73
$K^- e^\pm \mu^\mp$	0.22	0.26	1.88	2.18
$\bar{K}^{*0} e^\pm \mu^\mp$	1.24	0.67	1.63	3.15

TABLE III. The shape variable cuts determined from MC analysis, and the efficiency and the number of expected background events with those cuts.

mode	cuts	efficiency	$N_{\rm background}$			
		(3BPS)	from $B\bar{B}$		from $q\bar{q}$	
			correct	fake	correct	fake
$K^- e^+ e^-$	$R_2 < 0.45,\ \lvert\cos\theta_{\rm T}\rvert < 0.9,\ S_\perp > 0.2$	0.242	0.30	0.02	0.26	0.08
$\bar{K}^{*0} e^+ e^-$	$R_2 < 0.35$	0.098	0.76	0.09	0.05	0.08
$K^- \mu^+ \mu^-$	$R_2 < 0.35,\ \lvert\cos\theta_{\rm T}\rvert < 0.8$	0.151	0.26	0.17	0.03	0.18
$\bar{K}^{*0} \mu^+ \mu^-$	$R_2 < 0.35$	0.050	0.28	0.28	0.02	0.29
$K^- e^\pm \mu^\mp$	$R_2 < 0.3,$	0.240	0.16	0.17	0.04	0.10
$\bar{K}^{*0} e^\pm \mu^\mp$	$R_2 < 0.25$	0.084	0.48	0.41	0.04	0.16

TABLE IV. The upper limits on the branching ratios of various FCNC decay modes compared with previous best limits and the predictions from the Standard Model.

decay mode	N_{observed}	$N_{\text{background}}$ expected	upper limits (90%) this analysis	upper limits (90%) PDG-92 [11]	SM prediction [5]
$K^- e^+ e^-$	2	0.66	1.2×10^{-5}	5.0×10^{-5}	6.0×10^{-7}
$\bar{K}^{*0} e^+ e^-$	0	0.98	1.6×10^{-5}	2.9×10^{-4}	5.6×10^{-6}
$K^- \mu^+ \mu^-$	0	0.64	0.9×10^{-5}	1.5×10^{-4} [12]	6.0×10^{-7}
$\bar{K}^{*0} \mu^+ \mu^-$	0	0.87	3.1×10^{-5}	2.3×10^{-5}	2.9×10^{-6}
$K^- e^\pm \mu^\mp$	2	0.47	1.2×10^{-5}	$2 \times 6.4 \times 10^{-3}$	0
$\bar{K}^{*0} e^\pm \mu^\mp$	1	1.09	2.7×10^{-5}	$--$	0

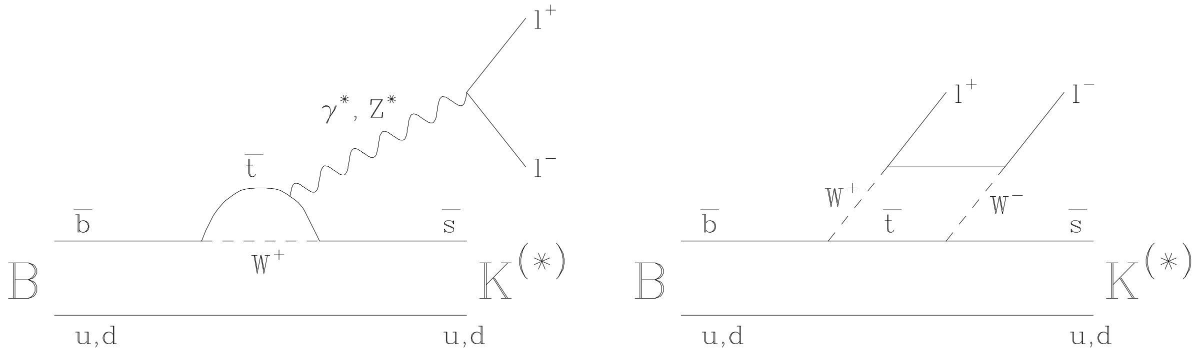

FIG. 1. Feynman diagrams of electroweak penguin and box decays.

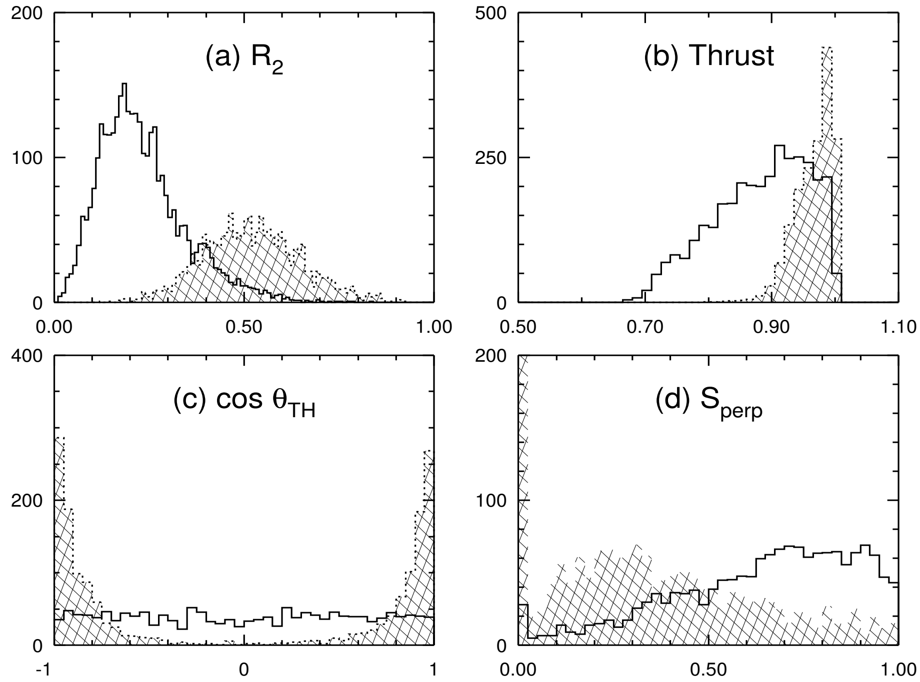

FIG. 2. Shape variable distributions for $q\bar{q}$ continuum MC (hatched histogram) and signal MC events (solid histogram) in the $K^-e^+e^-$ mode. The signal MC events are selected in the (M_B, ΔE) signal region, while the $q\bar{q}$ MC events are chosen in the wider (M_B, ΔE) region to compensate for the lack of statistics: (a) R_2, (b) thrust of the B candidate; and if thrust > 0.9, (c) $\cos\theta_{\mathrm{T}}$ and (d) $S_\perp$.

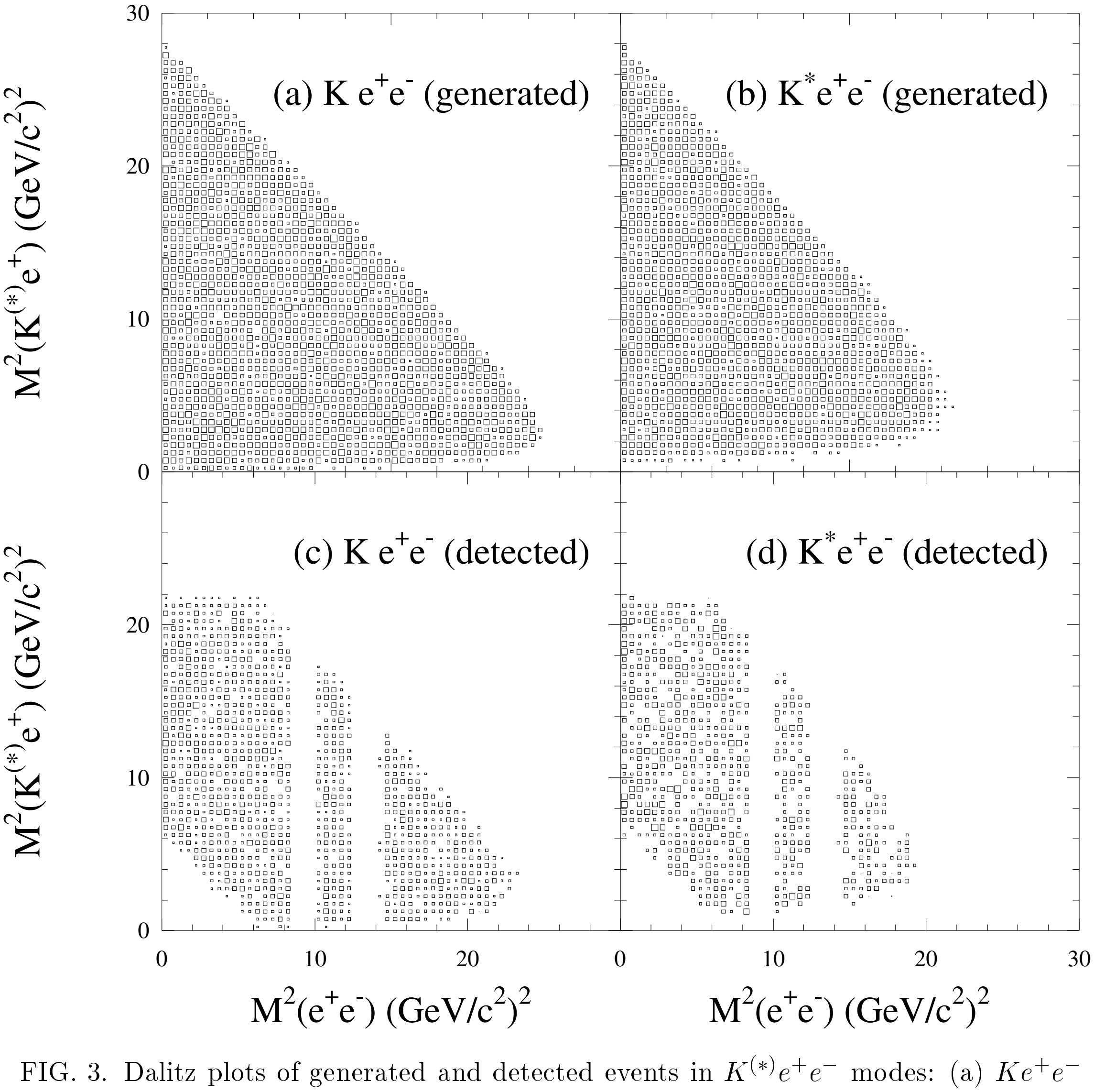

FIG. 3. Dalitz plots of generated and detected events in $K^{(*)}e^+e^-$ modes: (a) Ke^+e^- generated, (b) $K^*e^+e^-$ generated, (c) Ke^+e^- detected, and (b) $K^*e^+e^-$ detected.

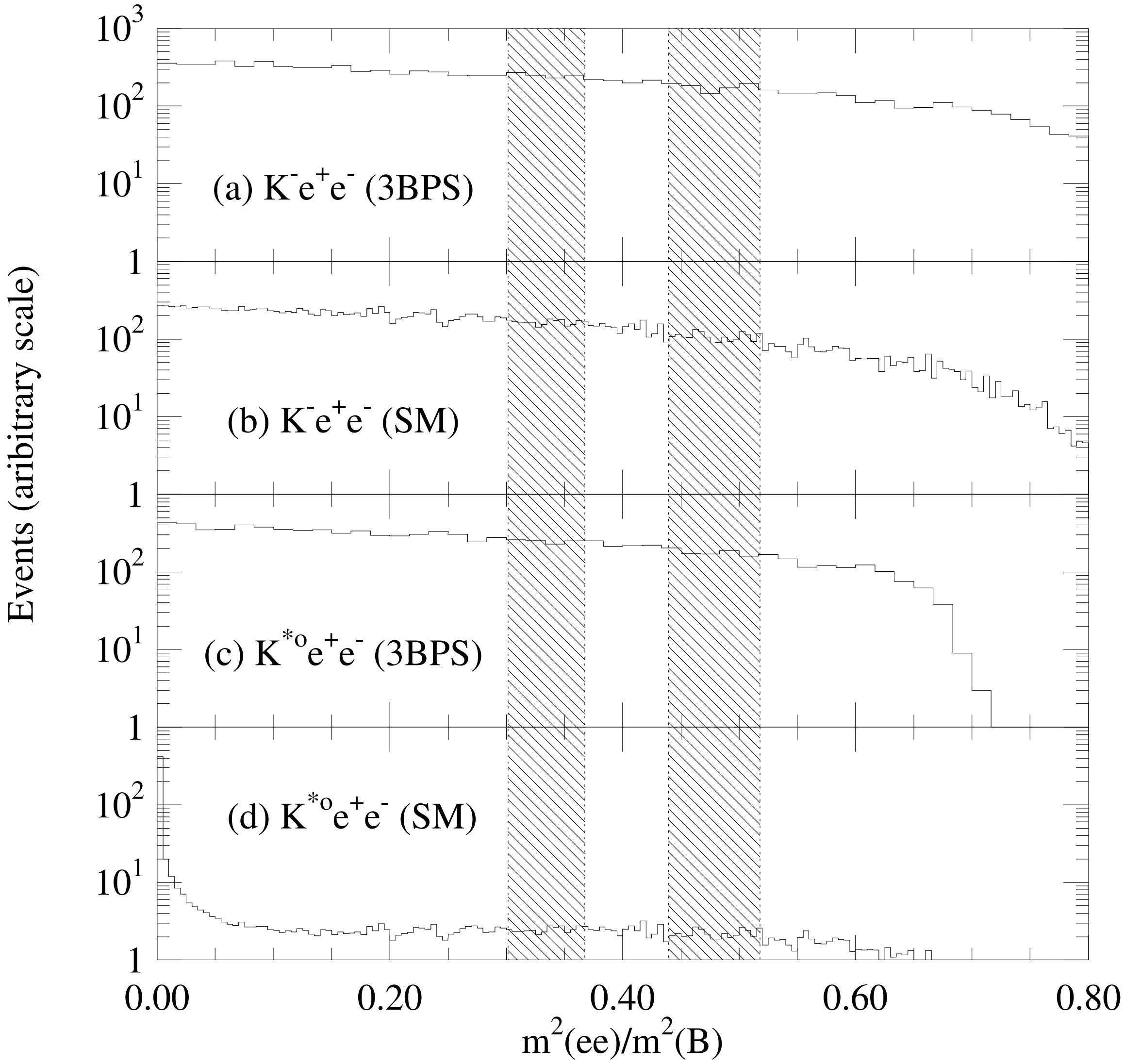

FIG. 4. Distribution of m_{ee}^2/m_B^2 as generated by MC using a 3-body-phase-space model (3BPS) and a Standard-Model-based phenomenological model (SM) by Ali *et al.* [4]: (a) $B^- \to K^- e^+ e^-$ (3BPS); (b) $B^- \to K^- e^+ e^-$ (SM); (c) $\bar{B}^0 \to \bar{K}^{*0} e^+ e^-$ (3BPS); and (d) $\bar{B}^0 \to \bar{K}^{*0} e^+ e^-$ (SM). The hatched area shows regions removed by ψ and ψ' veto.

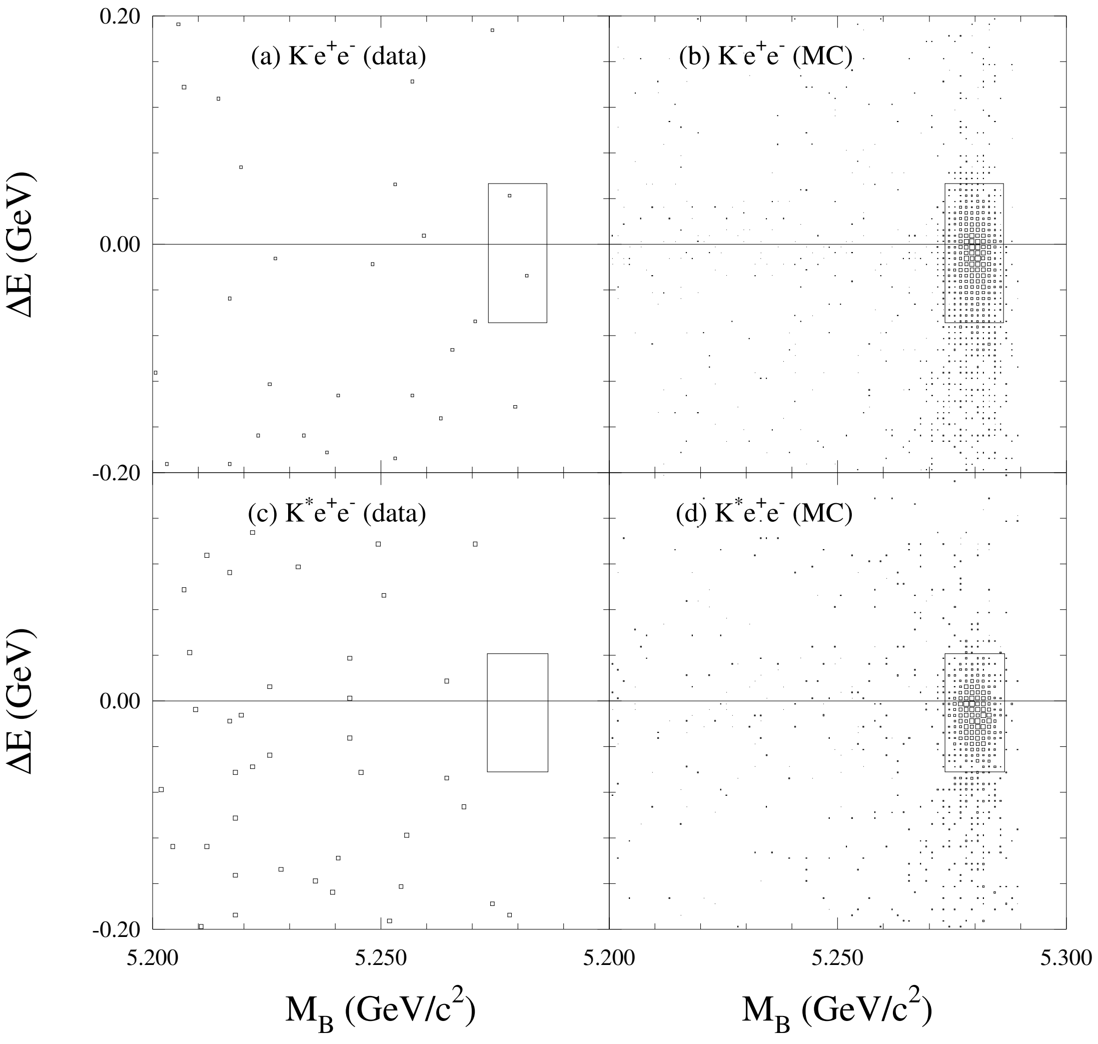

FIG. 5. Scatter plots of ΔE *vs.* M_B for $K^- e^+ e^-$ and $\bar{K}^{*0} e^+ e^-$ modes: (a) CLEO data for $K^- e^+ e^-$; (b) Signal MC for $K^- e^+ e^-$; (c) CLEO data for $\bar{K}^{*0} e^+ e^-$; (d) Signal MC for $\bar{K}^{*0} e^+ e^-$.

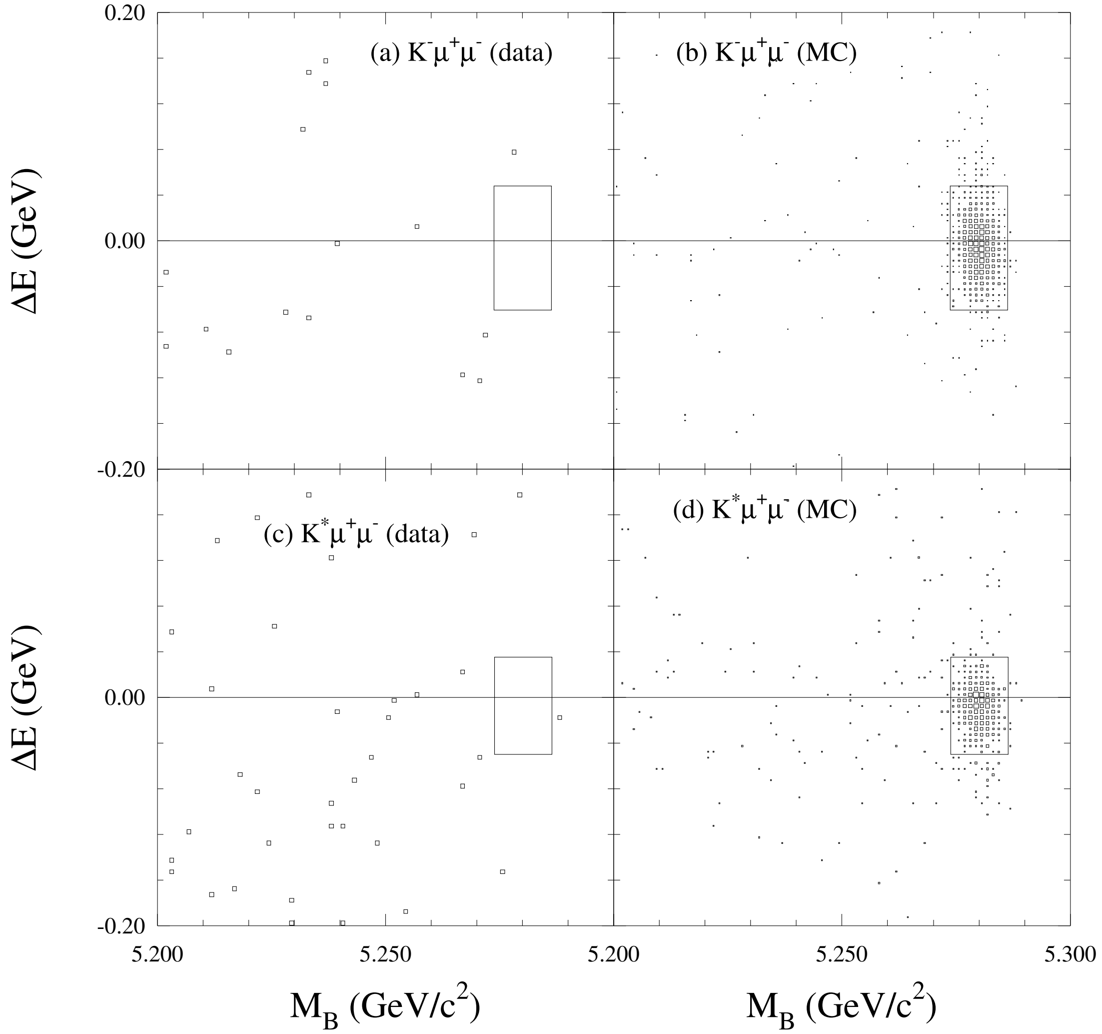

FIG. 6. Scatter plots of ΔE *vs.* M_B for $K^-\mu^+\mu^-$ and $\bar{K}^{*0}\mu^+\mu^-$ modes: (a) CLEO data for $K^-\mu^+\mu^-$; (b) Signal MC for $K^-\mu^+\mu^-$; (c) CLEO data for $\bar{K}^{*0}\mu^+\mu^-$; (d) Signal MC for $\bar{K}^{*0}\mu^+\mu^-$.

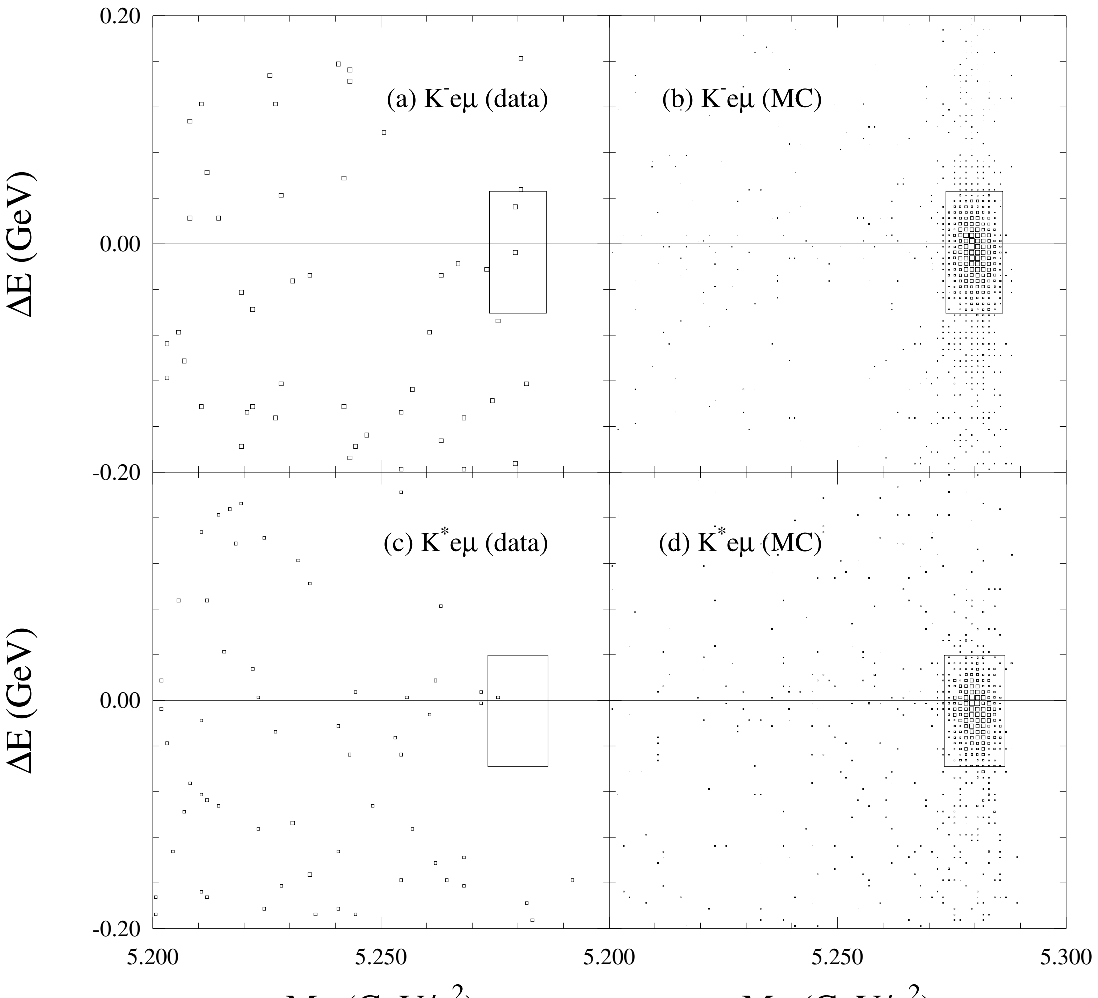

FIG. 7. Scatter plots of ΔE *vs.* M_B for $K^- e^\pm \mu^\mp$ and $\bar{K}^{*0} e^\pm \mu^\mp$ modes: (a) CLEO data for $K^- e^\pm \mu^\mp$; (b) Signal MC for $K^- e^\pm \mu^\mp$; (c) CLEO data for $\bar{K}^{*0} e^\pm \mu^\mp$; (d) Signal MC for $\bar{K}^{*0} e^\pm \mu^\mp$.